EISSN: 2231-0916 doi: 10.14202/vetworld.2026.4951-4969 OPEN ACCESS

Veterinary World

RESEARCH ARTICLE

Metabolite profiling and antimalarial activity of *Azadirachta indica* leaf extract: An integrated *in vivo* and *in silico* investigation

Dewa Ayu Agus Sri Laksemi[1], Putu Indah Budi Apsari[2], Made Bayu Permasutha[3], I Gusti Kamasan Nyoman Arijana[4], I Ketut Tunas[5] and I Made Agus Gelgel Wirasuta[6]

1. Department of Parasitology, Faculty of Medicine, Universitas Udayana, Denpasar, Bali 80234, Indonesia.
2. Department of Microbiology and Parasitology, Faculty of Medicine and Health Sciences, Warmadewa University, Denpasar, Bali 80235, Indonesia.
3. Division of Parasitology, Department of Biomedical Sciences, Faculty of Medicine, Universitas Pendidikan Ganesha, Bali 81116, Indonesia.
4. Department of Histology, Faculty of Medicine, Universitas Udayana, Denpasar, Bali 80234, Indonesia.
5. Health Information Management Study Program, Bali International University, Denpasar, Bali 80239, Indonesia.
6. Department of Pharmacy, Faculty of Mathematics and Natural Sciences, Universitas Udayana, Badung, Bali 80361, Indonesia.

ABSTRACT

Background and Aim: Antimalarial drug resistance highlights the need to identify alternative bioactive compounds. *Azadirachta indica* (neem) contains phytochemicals with potential antiplasmodial properties, although their molecular interactions remain incompletely characterized. This study aimed to characterize the metabolites of *A. indica* leaf extract, evaluate its antimalarial activity against *Plasmodium berghei*, and investigate predicted interactions between selected metabolites and parasite-associated proteins.

Materials and Methods: Ethanolic leaf extract was characterized using liquid chromatography–high-resolution mass spectrometry (LC-HRMS). Twenty-five male BALB/c mice infected with chloroquine-sensitive *P. berghei* ANKA were randomly assigned to five groups (n = 5). Three groups received oral extract doses of 250, 500, or 750 mg/kg body weight for four consecutive days. Artesunate (2.4 mg/kg) and distilled water served as positive and negative controls, respectively. Parasitemia suppression was evaluated using a modified Peters' 4-day suppressive test. Selected metabolites underwent molecular docking against *Plasmodium falciparum* dihydrofolate reductase–thymidylate synthase, chloroquine resistance transporter, and plasmepsin II, alongside exploratory host-response targets caspase-3 and Bcl-2. Molecular dynamics simulations (100 ns) and binding free-energy calculations assessed predicted interaction stability.

Results: LC-HRMS tentatively identified 33 metabolites, predominantly flavonols and flavonol glycosides. Scopoletin exhibited the greatest relative abundance, followed by rutin, trifolin, isoquercetin, quercetin 3-β-D-glucoside, and morin. Parasitemia suppression reached 78.11%, 82.08%, and 76.83% at 250, 500, and 750 mg/kg, respectively, compared with 95.75% for artesunate. The highest numerical suppression occurred at 500 mg/kg. Differences among extract-treated and artesunate groups were not statistically significant ($p > 0.05$), although therapeutic equivalence was not established. Computational analyses identified favorable predicted interactions involving catechin, luteolin, and 2-coumaroylquinic acid, particularly luteolin with the chloroquine resistance transporter.

Conclusion: *A. indica* leaf extract demonstrated preliminary antimalarial activity against chloroquine-sensitive *P. berghei*. Integrated metabolite profiling and computational analyses identified candidate compounds warranting further investigation. Experimental target validation, individual-compound testing, and evaluation against drug-resistant parasites are necessary to establish mechanisms and therapeutic relevance.

Keywords: *Azadirachta indica*, antimalarial activity, liquid chromatography–high-resolution mass spectrometry, molecular docking, molecular dynamics, neem leaf extract, *Plasmodium berghei*, phytochemical profiling.

INTRODUCTION

Malaria remains a major global public health threat, with more than 200 million cases reported annually [1]. Although artemisinin-based combination therapies (ACTs) remain central to malaria treatment, drug-resistant *Plasmodium* strains continue to emerge and spread, posing substantial challenges to malaria control and

Corresponding Author: Dewa Ayu Agus Sri Laksemi
E-mail: srilaksemi@unud.ac.id

Received: 12-06-2026, **Accepted:** 02-10-2026, **Published online:** 04-11-2026

Co-authors: PIBA: putuindah51@yahoo.com; MBP: bayu.permasutha@undiksha.ac.id; IGKNA: nyomanarijana@unud.ac.id; IKT: tunas@unbi.ac.id; IMAGW: gelgel.wirasuta@unud.ac.id

How to cite: Laksemi DAAS, Apsari PIB, Permasutha MB, Arijana IGKN, Tunas IK, Wirasuta IMAG. Metabolite profiling and antimalarial activity of *Azadirachta indica* leaf extract: An integrated in vivo and in silico investigation. Vet World. 2026;19(11):4951–4969.

Copyright: Laksemi *et al*. This article is an open access article distributed under the terms of the Creative Commons Attribution 4.0 International License (https://creativecommons.org/licenses/by/4.0/).

underscoring the need to identify alternative antimalarial compounds and therapeutic targets [2]. Medicinal plants represent a potential source of bioactive compounds, and *Azadirachta indica* (neem) has a history of traditional use in malaria treatment [3]. However, investigations of medicinal plants have frequently focused on crude extracts without comprehensive chemical characterization, limiting the identification of individual constituents potentially responsible for their observed biological activities [4].

Advances in analytical technologies, particularly liquid chromatography–high-resolution mass spectrometry (LC-HRMS), have facilitated the comprehensive profiling and tentative identification of plant-derived metabolites [5]. Integrating LC-HRMS with *in silico* approaches, including molecular docking, molecular dynamics (MD) simulations, and molecular mechanics/generalized Born surface area (MM/GBSA) or membrane adapted MM/PBSA calculations, provides a complementary framework for investigating the predicted molecular interactions, binding affinities, and conformational stability of candidate compounds [6]. These approaches can facilitate the prioritization of metabolites for further investigation against established *Plasmodium* targets [7], including dihydrofolate reductase–thymidylate synthase (PfDHFR-TS) [8, 9], plasmepsin II (PMII) [10], and the chloroquine resistance transporter (PfCRT) [11]. Nevertheless, computationally predicted binding affinities and interaction patterns do not independently establish biological activity, experimentally confirmed target engagement, or a compound's mechanism of action.

Beyond parasite-directed targets, host-response pathways may provide complementary information regarding the potential biological interactions of plant-derived metabolites. Caspase-3 and Bcl-2 participate in apoptotic regulation through distinct mechanisms. Caspase-3 functions as a downstream executioner of apoptosis, whereas Bcl-2 is an anti-apoptotic regulator associated with the mitochondrial apoptotic pathway [12, 13]. Accordingly, these proteins were included as exploratory host-response targets to investigate the predicted interactions of selected *A. indica* metabolites with proteins involved in apoptotic regulation. However, computational predictions alone cannot establish whether these metabolites modulate apoptosis or confer host-tissue protection under experimental conditions.

Previous investigations have demonstrated the antiplasmodial potential of *A. indica* leaf extracts. Rahmah *et al.* [4] reported parasitemia suppression ranging from 67.06% to 73.27% following administration of *A. indica* leaf extract at doses of 320-640 mg/kg. Although these findings support the potential antimalarial activity of the crude extract, they do not establish which individual metabolites contribute to the observed effects or identify the parasite-associated proteins potentially involved. Furthermore, previous investigations have frequently emphasized either experimental evaluation of crude extracts or computational assessment of selected phytochemicals against individual molecular targets. Consequently, the integration of comprehensive metabolite profiling, comparative multi-target computational analysis, and experimental antimalarial evaluation remains an important area for further investigation.

Another limitation of studies investigating crude botanical extracts is the difficulty of linking observed biological effects to specific chemical constituents when metabolite characterization and biological testing are performed independently. Differences in phytochemical composition may complicate the interpretation and comparison of experimental findings. Characterizing a defined extract and evaluating its biological activity alongside the predicted molecular interactions of its constituent metabolites may therefore provide a more coherent framework for identifying candidate antimalarial compounds. In particular, integrating chemical profiling with computational assessment of multiple parasite-associated proteins can help prioritize metabolites for subsequent experimental investigation without assuming that favorable predicted binding affinities establish biological efficacy.

Furthermore, the relationship between predicted parasite-directed interactions and potential host-response effects remains insufficiently characterized within this experimental framework. Although proteins involved in apoptotic regulation may provide additional exploratory targets, computational interactions with these proteins cannot establish functional modulation of apoptosis or protection against malaria-associated tissue injury. Similarly, antimalarial activity demonstrated in a chloroquine-sensitive rodent malaria model cannot establish efficacy against drug-resistant parasites or human malaria. These considerations highlight the need for an integrated investigation that distinguishes experimentally observed antimalarial activity from computationally predicted molecular interactions while identifying specific questions for subsequent mechanistic validation.

This study aimed to characterize the phytochemical composition and evaluate the antimalarial activity of *A. indica* leaf extract collected in Gianyar, Bali, Indonesia, through an integrated experimental and computational approach. The investigation combined chemical characterization, multi-target molecular modeling, and experi-

mental evaluation of the same extract to generate complementary evidence regarding its antimalarial potential.

Specifically, the study sought to (1) characterize the major metabolites of the ethanolic leaf extract using LC-HRMS; (2) evaluate the predicted binding affinities and interaction patterns of selected metabolites against PfDHFR-TS, PMII, and PfCRT through molecular docking; (3) investigate the conformational stability and predicted binding free energies of selected protein–ligand complexes using 100-ns MD simulations, with caspase-3 and Bcl-2 included as exploratory host-response targets; and (4) determine the *in vivo* antimalarial activity of the extract by measuring parasitemia suppression in mice infected with *Plasmodium berghei*.

By integrating these complementary approaches, the study sought to characterize the chemical constituents of a defined *A. indica* extract, document its experimental antimalarial activity, and prioritize selected metabolites for subsequent investigation of their potential molecular targets. The computational analyses involving caspase-3 and Bcl-2 were exploratory and were not designed to demonstrate modulation of host apoptosis. Because apoptosis-related biomarkers, pathway-specific assays, and experimental target-validation studies were not performed, the predicted molecular interactions were interpreted as hypothesis-generating findings rather than evidence of established antimalarial mechanisms. The findings were intended to provide a foundation for further investigation of individual metabolites, experimental target engagement, and antimalarial activity against drug-resistant parasites.

MATERIALS AND METHODS

Ethical approval

The study was approved by the Research Ethics Committee of the Faculty of Medicine, Universitas Udayana (Protocol No. 2073/UN14.2.2.VII.14/LT/2025). The approved study involved experimental infection of laboratory mice with a rodent malaria parasite, administration of the test extract and control treatments, and collection of blood samples for parasitemia assessment.

Study period and location

This study was conducted from January to December 2025 at several research facilities in Bali and Yogyakarta, Indonesia. *A. indica* leaves were collected in Gianyar, Bali, Indonesia, and the *P. berghei* ANKA strain was obtained from the Faculty of Medicine, Brawijaya University, Indonesia. The study involved plant extraction and chemical characterization, computational evaluation of selected metabolites, and experimental assessment of antimalarial activity. Plant extraction was performed at the Faculty of Pharmacy, Universitas Mahasaraswati Denpasar, Bali, Indonesia. Liquid chromatography–high-resolution mass spectrometry (LC-HRMS) analysis was conducted at PT Wiralab Analitika Solusindo and Corpora Science, Yogyakarta, Indonesia. *In silico* analyses, including molecular docking and molecular dynamics simulations, were performed at the Faculty of Medicine, Universitas Pendidikan Ganesha, Bali, Indonesia. *In vivo* animal experiments were carried out at the Integrated Biomedical Laboratory, Faculty of Medicine, Universitas Udayana, Bali, Indonesia.

Study design

An integrated experimental and computational design was used to characterize the metabolites of *A. indica* leaf extract and evaluate its antimalarial activity. A single homogenized batch of extract was prepared and used for LC-HRMS profiling and *in vivo* antimalarial evaluation to maintain consistency between the chemically characterized material and the material administered to the experimental animals.

The computational component comprised pharmacokinetic and toxicity screening, molecular docking, MD simulations, and binding free-energy calculations. The *in vivo* component involved 25 male BALB/c mice infected with chloroquine-sensitive *P. berghei* ANKA. The mice were randomly allocated to five groups (n = 5 per group), comprising three extract-treated groups and positive and negative control groups. Antimalarial activity was evaluated by determining parasitemia and parasitemia suppression after four consecutive days of treatment.

Metabolomic profiling using LC-HRMS

Preparation of the leaf extract and analytical sample: Neem leaves were collected from Pejeng Gianyar Bali and botanically authenticated by a qualified botanist (Ni Made Gari) at Universitas Udayana, Bali, Indonesia, prior to extraction. The extraction process was conducted at room temperature for 24 h. The extraction yield was calculated by dividing the weight of the concentrated crude extract by the initial weight of the dried plant material and multiplying the result by 100. The extraction yield was expressed as a percentage (%).

Dried *A. indica* plant material (128 g) was extracted using 1,280 mL of 80% aqueous s ethanol (Onemed; PT Jayamas Medica Industri Tbk; Sidoarjo Indonesia) (v/v), maintaining a plant material-to-solvent ratio of 1:10 (w/v).

The extraction yield was 12.1%.

For LC-HRMS analysis, a 10-mg aliquot of the stored extract was reconstituted in 1 mL of 80% methanol (LC-MS grade; Fisher Chemicals, Fisher Scientific, Fair Lawn, NJ, USA; Cat. No. A456-212) to obtain a final concentration of 10 mg/mL. The mixture was vortexed at 3,000 rpm for 2 min using a Thermo Scientific vortex mixer and sonicated at 40 kHz for 30 min in a PS-30A ultrasonic bath. The solution was subsequently centrifuged at 1,400 × *g* for 10 min using an Eppendorf Centrifuge 5425R. The supernatant was filtered through a 0.20 µm nylon membrane into an LC-MS vial for subsequent analysis.

Chromatographic conditions: Chromatographic separation was performed using a Thermo Scientific Vanquish Horizon ultra-high-performance liquid chromatography system equipped with a binary pump (Germering, Germany) and a Thermo Scientific Accucore C18 analytical column (100 mm × 2.1 mm internal diameter; 2.6-µm particle size; Lithuania).

The mobile phase consisted of mass spectrometry-grade water containing 0.1% formic acid (Optima™ LC/MS grade; 50 mL; Cat. No. A117-50) were obtained from Fisher Chemical™ (solvent A) and mass spectrometry-grade acetonitrile (2.5 L; Cat. No. A955-212) containing 0.1% formic acid (solvent B). Separation was performed at a flow rate of 0.3 mL/min over a total run time of 25 min. The gradient began at 5% solvent B, increased to 90% over 16 min, remained at 90% for 4 min, and returned to 5% for the remainder of the run. The column temperature was maintained at 40 °C, and the injection volume was 5 µL.

Mass spectrometric conditions and metabolite annotation

High-resolution mass spectrometric detection was performed using a Thermo Scientific Orbitrap Exploris 240 mass spectrometer (Bremen, Germany), operated in full-scan/data-dependent tandem mass spectrometry (Full MS/dd-MS^2) acquisition mode with polarity switching. Full-scan spectra were acquired at a resolution of 60,000 full width at half maximum over an *m/z* range of 67–1000, with a maximum injection time of 100 ms.

Precursor ion selection was based on an intensity threshold of 5,000, a charge state of 1, and a mass tolerance of 5 ppm. Data-dependent tandem mass spectra were acquired at a resolution of 30,000 using normalized collision energies of 30, 50, and 70, with nitrogen as the collision gas.

Ionization was performed using an OptaMax NG heated electrospray ionization source. Spray voltages were 3,500 V in positive-ion mode and 2,500 V in negative-ion mode. Sheath, auxiliary, and sweep gas settings were 35, 7, and 1 arbitrary units, respectively. The ion transfer tube and vaporizer temperatures were maintained at 300 °C and 320 °C, respectively.

Data were processed using Compound Discoverer version 3.5 (Thermo Scientific, San Jose, USA). Metabolites were tentatively annotated by spectral matching against the mzCloud library. The search prioritized the endogenous metabolites (12,346 entries), natural products/medicines (1,337 entries), and natural toxins (49 entries) categories. Metabolite annotations were retained only when the spectral match score was ≥95%.

***In silico* evaluation of absorption, distribution, metabolism, excretion, and toxicity**

The pharmacokinetic and toxicity profiles of metabolites identified by LC-HRMS were predicted computationally. Simplified molecular-input line-entry system (SMILES) representations were retrieved from PubChem. Absorption, distribution, metabolism, and excretion (ADME) parameters and drug-likeness were evaluated using SwissADME. Compounds with no violations of Lipinski's rule of five were prioritized.

Predicted toxicity was evaluated using ProTox 3.0 (https://tox.charite.de/protox3), which categorizes compounds into six toxicity classes according to estimated oral median lethal dose (LD_{50}) values. Only compounds assigned to toxicity classes IV–VI, corresponding to predicted oral LD_{50} values greater than 300 mg/kg, were selected for subsequent computational analysis. These classifications were used as computational screening criteria rather than evidence of experimentally established safety.

Molecular docking

Molecular docking was performed using AutoDock Vina version 1.2.7 (https://vina.scripps.edu) in an Ubuntu environment running under Windows Subsystem for Linux (WSL). The ligand library comprised compounds selected through preliminary ADME, toxicity, and drug-likeness screening, with artemisinin included as the reference compound.

Ligand structures were obtained as three-dimensional SDF or MOL2 files and prepared using Meeko version 0.7.1 (https://github.com/forlilab/Meeko), which generated PDBQT files with assigned atom types and Gasteiger partial charges. Protein receptors were similarly prepared in PDBQT format using Meeko version 0.7.1 with default receptor charge assignments.

Docking configurations were adapted to the structural characteristics of the individual targets. For the PfDHFR-TS holo-receptor system (Protein Data Bank [PDB] ID: 1J3I), the nicotinamide adenine dinucleotide phosphate (NADPH) cofactor was retained as part of the receptor. NADPH was converted into rigid PDBQT format using Open Babel version 2.4.1 (https://openbabel.org), assigned Gasteiger partial charges, and merged with the protein structure. The cofactor remained rigid and was excluded from active docking. The search box encompassed the region surrounding NADPH to permit ligand interactions within the extended binding site.

For the caspase-3 protein–protein interface system (PDB ID: 2XYG), the receptor comprised chains A and B. The search box encompassed the cavity formed between these chains. For PMII (PDB ID: 4YA8), Bcl-2 (PDB ID: 6GL8), and PfCRT (PDB ID: 6UKJ), the search boxes were centered on the designated binding sites and sized to enclose the corresponding binding pockets.

The exhaustiveness parameter was set to 20 for all calculations. Up to 10 binding poses were generated per ligand and ranked according to predicted binding affinity. Alternative poses were retained within an energy range of 3 kcal/mol relative to the best-scoring pose.

The predicted binding affinity of the top-ranked conformation (pose 1) was recorded for each ligand. Docking results were exported in SDF and PDB formats for three-dimensional visualization and interaction analysis using BIOVIA Discovery Studio version 21 (https://discover.3ds.com/discovery-studio-visualizer-download).

Ligand-efficiency (LE) was calculated to normalize predicted binding affinity according to ligand size [14]:

$$\mathrm{LE} = \frac{-\Delta G}{\mathrm{HA}}$$

where ΔG represents the AutoDock Vina docking score (kcal/mol), used as an approximate binding free-energy estimate, and HA represents the number of heavy atoms in the ligand. More negative docking scores indicate more favorable predicted binding, whereas LE is reported as a positive value for favorable negative scores, in kcal mol^{-1} per heavy atom.

The docking-derived estimate of the inhibition constant (K_i) was calculated using the following thermodynamic relationship:

$$K_i = C^{\circ} \exp[\frac{\Delta G}{RT}]$$

where C° is the standard concentration of 1 mol L^{-1}, R is the ideal gas constant (0.0019872041 kcal mol^{-1} K^{-1}), and T is the temperature (298.15 K). The docking score retained its original negative sign in this calculation. K_i values were calculated in molar units and converted to nM or μM for presentation.

The corresponding estimated pK_i was calculated as:

$$pK_i = -\log_{10}(\frac{K_i}{C^{\circ}})$$

Size-independent ligand efficiency (SILE) was calculated from the estimated pK_i using the heavy-atom normalization proposed by Nissink [14];

$$\mathrm{SILE} = \frac{pK_i}{HA^{0.3}}$$

Because K_i and pK_i were derived from docking scores rather than experimental inhibition data, these values were interpreted exclusively as computational estimates for comparative purposes. Docking-derived K_i is not an experimentally measured inhibition constant and does not establish inhibitory potency or mechanism.

MD simulations

Simulation systems and force-field preparation: MD simulations were performed using GROMACS version 2026.0 in an Ubuntu environment running under WSL. The computational platform comprised an HP Victus laptop equipped with a 13th-generation Intel Core i7-13700HX processor, 32 GB of random-access memory, and an NVIDIA GeForce RTX 4060 laptop graphics processing unit with 8 GB of video memory. Graphics processing unit acceleration was used during production simulations.

Initial protein–ligand coordinates were obtained from the molecular docking results. Simulation protocols were adapted to the structural characteristics of each target.

For PfDHFR-TS (PDB ID: 1J3I), the simulated system comprised the protein–ligand complex with the NADPH cofactor retained. For PfCRT (PDB ID: 6UKJ), an all-atom membrane simulation was performed by embedding the

protein–ligand complex in a 1-palmitoyl-2-oleoyl-*sn*-glycero-3-phosphocholine (POPC) lipid bilayer. For caspase-3 (PDB ID: 2XYG), the receptor comprised the complete chain A–B assembly because the ligand-binding site was located at the protein–protein interface. PMII (PDB ID: 4YA8) and Bcl-2 (PDB ID: 6GL8) were simulated using conventional soluble protein–ligand protocols.

Protein structures were parameterized using the AMBER ff14SB force-field. Ligand parameters were generated using ACPYPE (AnteChamber PYthon Parser interfacE) through an AMBER-based parameterization workflow. Ligand topologies were prepared using the General AMBER Force-Field version 2 (GAFF2), with AM1-BCC partial atomic charges. The resulting ligand and protein parameters were combined to maintain force-field compatibility.

Solvation and membrane-system preparation: Soluble protein–ligand complexes were solvated with explicit TIP3P water molecules, neutralized using counterions, and adjusted to an ionic strength of 0.15 M. The PfDHFR-TS holo-receptor system retained both the ligand and NADPH throughout simulation. For the caspase-3 interface-binding system, the receptor was represented by the complete chain A–B assembly to preserve the interaction interface.

For the PfCRT membrane-system, the protein–ligand complex was embedded in a POPC lipid bilayer using PACKMOL-Memgen. The membrane was parameterized using the AMBER Lipid21 force-field, the protein using AMBER ff14SB, and the ligand using GAFF2 with AM1-BCC charges. The assembled system was solvated with TIP3P water, ionized, and adjusted to a salt concentration of 0.15 M. The AMBER topology generated during membrane construction was subsequently converted into a GROMACS-compatible format.

Simulation conditions: Following energy minimization, each system underwent 100 ps of equilibration under constant particle number, volume, and temperature (NVT), followed by two successive 100-ps equilibration stages under constant particle number, pressure, and temperature (NPT). Position restraints were enabled during NVT and the first NPT stage and released during the second NPT stage. Each complex subsequently underwent one 100-ns production simulation, without independent replicate simulations.

A 2-fs integration time step was used. Long-range electrostatic interactions were calculated using the particle mesh Ewald method, with a short-range Coulomb cutoff of 1.2 nm. For the nonmembrane systems, van der Waals interactions were force-switched between 1.0 and 1.2 nm. For the PfCRT membrane system, a van der Waals cutoff of 1.2 nm was used. Bonds involving hydrogen atoms were constrained using the LINCS algorithm.

The temperature was maintained at 310 K using the V-rescale thermostat. Pressure was maintained at 1 bar using C-rescale during the first NPT stage and Parrinello–Rahman during the second NPT stage and production. Isotropic pressure coupling was used for the nonmembrane systems, whereas semi-isotropic coupling was used for PfCRT. Coordinates were saved every 10 ps during production simulations of the nonmembrane systems.

Trajectory analysis

Simulation trajectories were analyzed to assess the structural stability and dynamic behavior of each protein–ligand complex. The evaluated parameters included protein and ligand root-mean-square deviation (RMSD), Cα residue root-mean-square fluctuation (RMSF), radius of gyration (Rg), solvent-accessible surface area (SASA), and protein–ligand hydrogen-bond interactions. Hydrogen bonds were evaluated using the analysis module implemented in GROMACS.

Binding free-energy calculations

Binding free energies were estimated using gmx_MMPBSA version 1.6.4 (https://valdes-tresanco-ms.github.io/gmx_MMPBSA/). For soluble protein–ligand systems, MM/GBSA calculations were performed using the generalized Born model specified by igb = 5 and a salt concentration of 0.15 M.

The same MM/GBSA settings were applied to the PfDHFR-TS holo-receptor and caspase-3 interface-binding systems, with receptor definitions adjusted according to their structural characteristics. The receptor was defined as the protein for conventional soluble protein–ligand complexes, the protein together with NADPH for PfDHFR-TS, and chains A and B for caspase-3.

For PfCRT, membrane-adapted molecular mechanics/Poisson–Boltzmann surface area (MM/PBSA) calculations were used because the protein was simulated within a POPC lipid bilayer. The membrane environment was represented as an implicit dielectric region during the Poisson–Boltzmann calculations. The membrane option was enabled (memopt = 1), with a membrane dielectric constant of 7.0, an internal dielectric constant of 1.0, a membrane thickness of 30 Å, and an ionic strength of 0.15 M.

For the nonmembrane systems, production trajectories were subsampled at 1-ns intervals, and the first 100 frames of the subsampled trajectories were selected for MM/GBSA calculations. The resulting binding-energy estimates were interpreted as comparative energetic trends rather than experimentally measured binding affinities.

Each complex was evaluated using a single 100-ns production trajectory, without independent replicate simulations. Consequently, the simulation-derived parameters and binding-energy estimates were interpreted as exploratory computational observations rather than definitive evidence of biological activity or ligand superiority.

In vivo antimalarial evaluation

Parasite strain and experimental animals: The antimalarial assays used chloroquine-sensitive *P. berghei* ANKA obtained from the Faculty of Medicine, Brawijaya University, Indonesia. Twenty-five male BALB/c mice, aged 8 weeks and weighing 25–30 g, were acclimatized for 1 week under a controlled 12-h light/dark cycle before the experiments.

Animals were monitored regularly throughout the experimental period for clinical signs of distress, changes in body weight, activity, posture, and food and water intake. Each mouse was infected by intraperitoneal injection of an inoculum containing 1 x 10^7 *P. berghei*. At the end of the experiment, the mice were euthanized under the approved institutional animal ethics protocol. Ketamine was administered intraperitoneally at a dose of 400 mg/kg body weight, followed by cervical dislocation performed by trained personnel. Death was confirmed following the procedure. All procedures were conducted in accordance with the approved institutional animal ethics protocol and applicable animal welfare guidelines.

The number of animals was determined using the resource equation method [15]. The mice were randomly allocated to five groups (n = 5 per group).

Experimental groups and treatment administration: The negative control (NC) group comprised infected mice receiving 0.2 mL of distilled water orally. The positive control (PC) group comprised infected mice receiving artesunate (Guillian Pharmaceutical Co., Ltd., China) at 2.4 mg/kg body weight by intraperitoneal injection.

Both control groups received the same handling procedures as the treatment groups. Distilled water was administered as the vehicle at a volume equivalent to that given to the treatment groups.

The experimental mice were assigned unique identification numbers and randomly allocated to the control and treatment groups using a simple randomization procedure. A computer-based random number generator was used to generate the allocation sequence, and the mice were assigned to the respective groups according to this sequence. The group allocation list was documented. Blinding was not performed in this study.

Continuous variables were summarized as means ± standard deviations (SD). Differences in parasitemia and percentage suppression among independent experimental groups at the prespecified assessment time point were analyzed using one-way analysis of variance (ANOVA), provided that the assumptions of normality and homogeneity of variance were reasonably satisfied. Tukey's post hoc test was used for pairwise comparisons when the ANOVA indicated a statistically significant difference. All statistical tests were two-sided, and a p-value of less than 0.05 was considered statistically significant. Statistical analyses were performed using IBM SPSS Statistics.

Three treatment groups received *A. indica* ethanolic leaf extract orally at doses of 250 mg/kg body weight (T1), 500 mg/kg body weight (T2), and 750 mg/kg body weight (T3), respectively.

The extract was administered by oral gavage at a fixed volume of 0.2 mL per mouse, using distilled water as the vehicle. The extract suspension was freshly prepared before administration, and the administered dose was calculated according to the individual body weight of each mouse.

Treatment began approximately 3 h after infection on day 0 (D0) and was administered once every 24 h at the same time for four consecutive days (D0, D1, D2, and D3).

Parasitemia assessment

On day 4 (D4), thin blood smears were prepared from tail-vein blood, fixed with absolute methanol (Merck Sigma-Aldrich, Darmstadt, Germany), and stained with 10% Giemsa solution (Giemsa's azur eosin methylene blue solution Merck Sigma-Aldrich) for 15 min. Parasitemia was assessed under a light microscope (Olympus CX21, Tokyo, Japan) using a 100× oil-immersion objective.

A minimum of 1,000 red blood cells (RBCs) were counted across five randomly selected microscopic fields per slide.

The percentage of parasitemia was calculated as follows [16]:

% Parasitemia = Number of infected RBCs/Total number of RBCs counted X 100

The mean percentage of parasitemia in each group was subsequently used to calculate parasitemia suppression using Peters' formula:

Mean percentage parasitemia suppression (PPS) = Mean PP in negative control-mean PP in treatment group/Mean PP in NC X 100

where PP represents percentage parasitemia.

RESULTS

Metabolomic profiling using LC-HRMS

LC-HRMS analysis of *A. indica* leaf extract revealed a complex phytochemical profile. The chromatogram contained multiple peaks, including a prominent peak attributed to scopoletin (Figure 1).

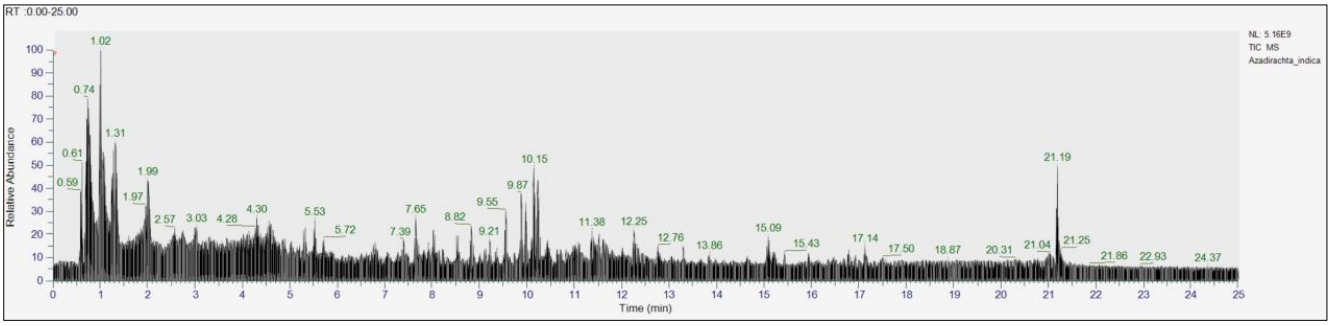


Figure 1: Liquid chromatography–high-resolution mass spectrometry chromatogram of *Azadirachta indica* leaf extract.

LC-HRMS analysis tentatively identified 33 metabolites (Table 1), including flavonols, flavonol glycosides, coumarins, phenolic compounds, and other phytochemical classes. Scopoletin had the largest reported peak area (4.33×10^9), followed by rutin, trifolin, isoquercetin, quercetin 3-β-D-glucoside, and morin. The reported mzCloud best-match scores ranged from 95.0% to 99.9%. These findings characterize the detected chemical constituents but do not independently establish the biological activity of individual metabolites.

Table 1: Tentative identification of compounds detected in *Azadirachta indica* by untargeted LC-HRMS.

Name	Formula	DeltaMass (ppm)	m/z	RT (min)	Reference ion	Polarity	Area	mzCloud best-match (%)	Phytochemical class
Scopoletin	C10H8O4	0.93	193.04971	4.438	[M+H]+	+	4331470736.10	98.4	Coumarin
Rutin	C27H30O16	0.74	611.16113	4.050	[M+H]+	+/-	2066710066.94	99.4	Flavonol glycoside
Trifolin	C21H20O11	0.57	449.10815	4.712	[M+H]+	+/-	1620408069.19	97.3	Flavonol glycoside
Isoquercetin	C21H20O12	0.32	465.10297	4.025	[M+H]+	+/-	1439267980.01	99.6	Flavonol glycoside
Quercetin 3-β-D-glucoside	C21H20O12	0.32	465.10297	4.163	[M+H]+	+/-	1439267980.01	99.6	Flavonol glycoside
Morin	C15H10O7	0.99	301.03568	6.026	[M-H]-	+/-	1116133975.17	99.3	Flavonol
Quercetin	C15H10O7	0.80	303.05017	4.265	[M+H]+	+	703826527.86	99.3	Flavonol
Kaempferol	C15H10O6	0.74	287.05524	4.575	[M+H]+	+/-	685932879.00	99.5	Flavonol
Quercetin-3-galactoside-7-rhamnoside	C27H30O16	0.73	609.14655	3.044	[M-H]-	-	449930269.05	99.7	Flavonol diglycoside
2-Hydroxy-5-[3,4,5-trihydroxy-6-(hydroxymethyl)oxan-2-yl]oxybenzoic acid	C13H16O9	0.93	315.07245	1.722	[M-H]-	-	408876776.02	97.5	Phenolic compound
Phlorizin	C21H24O10	0.46	435.12979	5.301	[M-H]-	+/-	311110089.45	99.9	Dihydrochalcone glycoside
Phloretin	C15H14O5	1.32	275.09177	5.298	[M+H]+	+/-	239730968.90	99.6	Dihydrochalcone
3',5'-di-C-glucosylphloretin	C27H34O15	0.80	597.18317	4.333	[M-H]-	+/-	209810302.70	99.6	Dihydrochalcone glycoside
Myricetin	C15H10O8	0.63	319.04504	3.734	[M+H]+	+	191855908.57	99.5	Flavonol
Trigonelline	C7H7NO2	–0.06	138.05495	0.865	[M+H]+	+	180061385.24	99.6	Alkaloid
Rhamnetin 3-galactoside	C22H22O12	0.39	479.11874	4.898	[M+H]+	+/-	174461808.36	95.0	Flavonol glycoside
Luteolin	C15H10O6	1.09	285.04080	6.901	[M-H]-	+/-	145328945.34	95.7	Flavone

Name	Formula	DeltaMass (ppm)	m/z	RT (min)	Reference ion	Polarity	Area	mzCloud best-match (%)	Phytochemical class
Isorhamnetin 3-robinobioside	C28H32O16	0.82	625.17676	4.585	[M+H]+	+/-	120977201.53	99.3	Flavonol glycoside
Quercitrin	C21H20O11	0.42	449.10803	4.335	[M+H]+	+/-	109124803.62	98.7	Flavonol glycoside
4-Hydroxybenzoic acid glucoside	C13H16O8	0.91	299.07751	2.591	[M-H]-	-	84846341.12	97.3	Phenolic compound
Isorhamnetin	C16H12O7	0.78	317.06583	4.897	[M+H]+	+	81654236.51	99.1	Flavonol
Catechin	C15H14O6	0.64	289.07199	3.323	[M-H]-	+/-	62570320.43	97.2	Flavan-3-ol
2-Coumaroylquinic acid	C16H18O8	0.55	337.09311	3.903	[M-H]-	+/-	50802220.50	96.7	Phenolic/organic acid derivative
(+)-Epicatechin	C15H14O6	0.96	289.07202	2.656	[M-H]-	+/-	48639577.41	97.3	Flavan-3-ol
4-Hydroxybenzoic acid	C7H6O3	0.75	137.02452	2.593	[M-H]-	-	42585248.77	96.5	Phenolic compound
Reynoutrin	C20H18O11	0.15	435.09238	4.503	[M+H]+	+/-	39306813.26	97.0	Flavonol glycoside
Epigallocatechin	C15H14O7	0.60	305.06693	2.297	[M-H]-	+/-	38333074.62	96.0	Flavan-3-ol
(+)-Gallocatechin	C15H14O7	0.44	305.06693	2.440	[M-H]-	+/-	35844551.28	96.0	Flavan-3-ol
Naringenin 4'-O-glucoside	C21H22O10	–0.02	433.11392	4.974	[M-H]-	+/-	35560100.11	97.9	Flavanone glycoside
Naringenin	C15H12O5	0.64	271.06137	6.934	[M-H]-	-	31272396.93	99.0	Flavanone
Kaempferol 3-robinobioside	C27H30O15	0.45	595.16602	4.227	[M+H]+	+	26323064.66	99.4	Flavonol glycoside
o-Hydroxyphenyl-beta-D-glucoside	C12H16O7	0.94	271.08258	2.496	[M-H]-	-	13643594.47	99.2	Phenolic glycoside
4-Hydroxy-2-(2-hydroxy-4-methoxy-6-propylbenzoyl)oxy-6-propylbenzoic acid	C21H24O7	–0.94	387.14456	11.612	[M-H]-	-	11388167.37	99.2	Phenolic compound

LC-HRMS = liquid chromatography–high-resolution mass spectrometry; ppm = parts per million; m/z = mass-to-charge ratio; RT = retention time; min = minutes; M = neutral molecule; [M+H]+ = protonated molecular ion; [M-H]- = deprotonated molecular ion; + = positive-ion mode; - = negative-ion mode; +/- = positive- and negative-ion modes. Peak area represents the reported chromatographic signal area.

Molecular docking

The target protein structures were obtained from the RCSB PDB. They comprised PfDHFR-TS (PDB ID: 1J3I), PfCRT (PDB ID: 6UKJ), PMII (PDB ID: 4YA8), caspase-3 (PDB ID: 2XYG), and Bcl-2 (PDB ID: 6GL8).

Docking sites were defined according to the positions of the co-crystallized reference ligands. The docking protocol was evaluated by redocking the reference ligands into their respective binding sites. All reported RMSD values were below 2 Å, ranging from 0.359 to 1.949 Å (Table 2).

Table 2: Binding site coordinates and validation results.

Parameter	1J3I (PfDHFR-TS)	6UKJ (PfCRT)	4YA8 (PMII)	2XYG (caspase-3)	6GL8 (Bcl-2)
Reference ligand	WRA	Y01	49W	TQ8	F3Q
Center x	27.287	145.945	–63.816	36.357	17.189
Center y	6.942	170.427	–23.911	38.829	2.647
Center z	58.548	141.210	–16.851	32.088	15.647
Size x	24	38	24	18	34
Size y	18	10	28	22	26
Size z	20	38	36	14	32
Redocking validation (Å)	1.547	1.949	0.616	0.932	0.359

PDB = Protein Data Bank; PfDHFR-TS = *Plasmodium falciparum* dihydrofolate reductase–thymidylate synthase; PfCRT = *Plasmodium falciparum* chloroquine resistance transporter; PMII = *Plasmodium falciparum* plasmepsin II; RMSD = root-mean-square deviation; Å = angstrom. Center x, y, and z indicate the docking-grid center coordinates; size x, y, and z indicate the corresponding grid dimensions.

Of the 33 tentatively identified metabolites, 14 compounds were selected for molecular docking based on the stated drug-likeness screening criteria, structural diversity, and biological relevance. The screening procedure excluded high-molecular-weight glycosides with molecular weights greater than 500 Da. The selected compounds were docked against five protein targets, with artemisinin included as a reference compound.

The docking results showed target-dependent variation in predicted binding affinities (Table 3). Among the screened metabolites, catechin had the most negative predicted binding energy for PfDHFR-TS (−8.672 kcal/mol), luteolin for PfCRT (−8.827 kcal/mol) and Bcl-2 (−6.927 kcal/mol), and 2-coumaroylquinic acid for PMII (−7.560 kcal/mol) and caspase-3 (−6.682 kcal/mol).

Several phytochemicals exhibited predicted binding energies within a similar numerical range to, or more negative than, those of artemisinin for particular targets. These findings indicate differences in computationally predicted ligand–target interactions but do not demonstrate biological inhibition or therapeutic superiority.

LE and related computational metrics were also evaluated to compare compounds with different molecular sizes. The docking-derived interaction properties of artemisinin and selected metabolites are presented in Table 4.

Table 3: Predicted binding affinities (kcal/mol) of screened ligands and artemisinin against five target proteins.

Ligands	1J3I (PfDHFR-TS)	6UKJ (PfCRT)	4YA8 (PMII)	2XYG (caspase-3)	6GL8 (Bcl-2)
Reference ligand	–9.365	–8.557	–8.444	–5.772	–11,130
Artemisinin	–8.197	–8.204	–6.520	–5.978	–6.731
Scopoletin	–7.497	–6.741	–5.738	–4.962	–5.418
Morin	–8.197	–8.553	–7.541	–6.401	–6.639
Kaempferol	–8.049	–8.234	–7.252	–6.289	–6.604
Phloretin	–8.417	–7.936	–6.739	–6.232	–6.344
Trigonelline	–5.451	–5.312	–4.674	–4.284	–4.824
Luteolin	–8.375	–8.827*	–7.537	–6.616	–6.927*
4-Hydroxybenzoic acid glucoside	–7.229	–7.404	–7.066	–6.231	–5.922
Isorhamnetin	–8.189	–8.406	–6.995	–6.585	–6.652
Catechin	–8.672*	–8.086	–7.079	–6.028	–6.391
2-Coumaroylquinic acid	–7.977	–7.602	–7.560*	–6.682*	–6.312
(+)-Epicatechin	–8.606	–8.563	–6.995	–5.986	–6.361
4-Hydroxybenzoic acid	–6.040	–5.299	–4.739	–4.369	–5.351
Naringenin	–8.287	–8.537	–7.360	–6.366	–6.720
o-Hydroxyphenyl-beta-D-glucoside	–6.830	–6.574	–6.435	–5.562	–5.760

PfDHFR-TS = *Plasmodium falciparum* dihydrofolate reductase–thymidylate synthase; PfCRT = *Plasmodium falciparum* chloroquine resistance transporter; PMII = *Plasmodium falciparum* plasmepsin II; kcal/mol = kilocalories per mole; ΔG = predicted binding energy. An asterisk indicates the ligand with the most negative predicted binding energy among the screened phytochemicals for the corresponding target. Values are computational predictions, not experimentally measured affinities.

Table 4: Key protein–ligand interactions observed from molecular docking of screened compounds.

Protein	Ligand	2D interaction diagram	Properties	Interacting residues
PfDHFR-TS (1J3I)	Artemisinin	Original diagram retained	ΔG: -8.197 kcal/mol; LE: 0.431; SILE: 2.484; Ki: 980.747 nM	Hydrogen bonds: none reported. Other interactions: Leu46, Met55, Phe58, Ile102, Pro103, Leu109, NADPH
PfDHFR-TS (1J3I)	Catechin	Original diagram retained	ΔG: -8.672 kcal/mol; LE: 0.413; SILE: 2.550; Ki: 439.926 nM	Hydrogen bonds: Asp54, Ser101, Tyr160. Other interactions: Ala16, Leu46, Phe58, Ile102, Ile154, NADPH
PfCRT (6UKJ)	Artemisinin	Original diagram retained	ΔG: -8.204 kcal/mol; LE: 0.432; SILE:2.486; Ki: 969.228 nM	Hydrogen bonds: Thr344. Other interactions: Tyr62, Tyr384, Leu385, Arg392
PfCRT (6UKJ)	Luteolin	Original diagram retained	ΔG: -8.827 kcal/mol; LE: 0.420; SILE: 2.596; Ki: 338.660 nM	Hydrogen bonds: Arg392, Asn395. Other interactions: Ile61, Thr344, Ile347, Val348, Tyr384, Arg392
PMII(4YA8)	Artemisinin	Original diagram retained	ΔG: -6.520 kcal/mol; LE: 0.343; SILE: 1.976; Ki: 16.627 μM	Hydrogen bonds: Asp34. Other interactions: Ile32, Tyr77, Val78
PMII (4YA8)	2-Coumaroylquinic acid	Original diagram retained	ΔG: -7.560 kcal/mol; LE: 0.315; SILE: 2.136; Ki: 2.874 μM	Hydrogen bonds: Asp34, Gly36, Gly216, Thr217. Other interactions: Gly36, Val78, Asp214, Phe294
Caspase-3 (2XYG)	Artemisinin	Original diagram retained	ΔG: -5.978 kcal/mol; LE: 0.315; SILE: 1.811; Ki: 41.505 μM	Hydrogen bonds: Thr62, Gly122. Other interactions: Met61, His121, Phe128, Cys163, Tyr204
Caspase-3 (2XYG)	2-Coumaroylquinic acid	Original diagram retained	ΔG: -6.682 kcal/mol; LE: 0.278; SILE: 1.888; Ki: 12.649 μM	Hydrogen bonds:Tyr204, Ser205, Arg207, Thr62, Thr59. Other interactions: Phe128, Met61
Bcl-2 (6GL8)	Artemisinin	Original diagram retained	ΔG: -6.731 kcal/mol; LE: 0.354; SILE:2.040; Ki: 11.645 μM	Hydrogen bonds: none reported. Other interactions: Phe112, Met115, Val133, Phe153
Bcl-2 (6GL8)	Luteolin	Original diagram retained	ΔG: -6.927 kcal/mol; LE: 0.330; SILE: 2.037; Ki: 8.365 μM	Hydrogen bonds: Ala100, Arg107. Other interactions: Phe104, Gly145, Arg146, Val148

PfDHFR-TS = *Plasmodium falciparum* dihydrofolate reductase–thymidylate synthase; PfCRT = *Plasmodium falciparum* chloroquine resistance transporter; PMII = *Plasmodium falciparum* plasmepsin II; PDB = Protein Data Bank; 2D = two-dimensional; ΔG = predicted binding energy; LE = ligand-efficiency; SILE = size-independent ligand-efficiency; Ki = estimated inhibition constant; NADPH = nicotinamide adenine dinucleotide phosphate; kcal/mol = kilocalories per mole; nM = nanomolar; μM = micromolar. Amino acid abbreviations: Ala = alanine; Arg = arginine; Asn = asparagine; Asp = aspartate; Cys = cysteine; Gly = glycine; His = histidine; Ile = isoleucine; Leu = leucine; Met = methionine; Phe = phenylalanine; Pro = proline; Ser = serine; Thr = threonine; Tyr = tyrosine; Val = valine.

The interaction profiles differed across the five targets. For PfDHFR-TS, catechin exhibited a more negative predicted binding energy than artemisinin and formed hydrogen bonds with Asp54, Ser101, and Tyr160. For PfCRT, luteolin exhibited a more negative predicted binding energy than artemisinin and formed hydrogen bonds with Arg392 and Asn395. For PMII, 2-coumaroylquinic acid exhibited a more negative predicted binding energy than artemisinin and formed hydrogen bonds with Asp34, Gly36, Gly216, and Thr217.

For the exploratory host-response targets, 2-coumaroylquinic acid exhibited a more negative predicted binding energy than artemisinin for caspase-3, while luteolin exhibited a slightly more negative predicted binding

energy than artemisinin for Bcl-2. These findings represent computationally predicted interactions and do not establish functional modulation of apoptosis.

The reported LE metrics provided additional descriptors for comparing compounds of different molecular sizes. Artemisinin exhibited relatively consistent atom-normalized efficiency across the evaluated targets, whereas luteolin showed a combination of favorable predicted binding energy and LE metrics for PfCRT. These comparisons were interpreted as computational trends rather than evidence of experimentally confirmed target inhibition.

MD simulations

The dynamic behavior of selected protein–ligand complexes was assessed using RMSD, RMSF, hydrogen-bond interactions, Rg, SASA, and binding free-energy estimates. The numerical results are presented in Table 5.

Table 5: Summary of molecular dynamics parameters and binding-energy estimates for selected protein–ligand complexes.

Protein–ligand	RMSD (Å), mean ± SD	RMSF (Å), mean ± SD	H-bond, mean ± SD	Rg (Å), mean ± SD	SASA (Å²), mean ± SD	Binding-energy estimate (kcal/mol), mean ± SD
1J3I-artemisinin	4.60 ± 1.49	1.63 ± 1.21	0.22 ± 0.42	18.50 ± 0.11	13302.32 ± 285.67	–22.63 ± 1.71
1J3I-catechin	4.29 ± 1.00	1.23 ± 0.97	1.26 ± 0.50	18.38 ± 0.14	13332.59 ± 247.78	–23.49 ± 2.82
6UKJ-artemisinin	5.36 ± 1.34	5.20 ± 2.26	0.63 ± 0.56	22.23 ± 0.15	20610.89 ± 555.47	–21.96 ± 1.09
6UKJ-luteolin	1.98 ± 0.65	3.00 ± 1.51	1.27 ± 0.66	21.90 ± 0.12	18929.71 ± 297.02	–26.16 ± 2.07
4YA8-artemisinin	20.34 ± 8.28	0.84 ± 0.46	0.52 ± 0.53	20.54 ± 0.09	15377.56 ± 211.39	–12.16 ± 0.5
4YA8-2-Coumaroylquinic acid	7.81 ± 1.68	0.93 ± 0.69	1.14 ± 0.63	20.51 ± 0.10	15485.52 ± 230.45	–14.83 ± 6.33
2XYG-artemisinin	2.68 ± 0.30	1.47 ± 0.86	0.27 ± 0.54	18.08 ± 0.11	12305.68 ± 269.18	–4.64 ± 1.4
2XYG-2-Coumaroylquinic acid	2.39 ± 0.23	1.02 ± 0.70	1.33 ± 1.18	18.03 ± 0.08	12064.94 ± 254.08	–11.15 ± 2.26
6GL8-artemisinin	6.13 ± 1.61	0.82 ± 0.40	0.24 ± 0.44	14.68 ± 0.06	8056.20 ± 176.22	–18.17 ± 1.32
6GL8-luteolin	7.85 ± 1.14	0.97 ± 0.47	0.78 ± 0.71	14.71 ± 0.07	8109.20 ± 174.60	–20.54 ± 0.35

RMSD = root-mean-square deviation; RMSF = root-mean-square fluctuation; H-bond = hydrogen-bond; Rg = radius of gyration; SASA = solvent-accessible surface area; SD = standard deviation; Å = angstrom; Å² = square angstrom; kcal/mol = kilocalories per mole. Protein Data Bank identifiers: 1J3I = *Plasmodium falciparum* dihydrofolate reductase–thymidylate synthase; 6UKJ = *Plasmodium falciparum* chloroquine resistance transporter; 4YA8 = *Plasmodium falciparum* plasmepsin II; 2XYG = caspase-3; 6GL8 = Bcl-2. Binding-energy estimates were calculated using membrane-adapted MM/PBSA for PfCRT (6UKJ) and MM/GBSA for the remaining systems. MM/PBSA = molecular mechanics/Poisson–Boltzmann surface area; MM/GBSA = molecular mechanics/generalized Born surface area.

Catechin exhibited lower mean RMSD (4.29 ± 1.00 Å) and RMSF (1.23 ± 0.97 Å) values than artemisinin (4.60 ± 1.49 Å and 1.63 ± 1.21 Å, respectively) in the PfDHFR-TS system. Catechin also showed a higher mean number of hydrogen bonds (1.26 ± 0.50 vs. 0.22 ± 0.42) and a slightly more negative MM/GBSA estimate (−23.49 ± 2.82 vs. −22.63 ± 1.71 kcal/mol).

For PfCRT, luteolin exhibited lower mean RMSD (1.98 ± 0.65 Å) and RMSF (3.00 ± 1.51 Å) values than artemisinin (5.36 ± 1.34 Å and 5.20 ± 2.26 Å, respectively). Luteolin also showed a higher mean number of hydrogen bonds (1.27 ± 0.66 vs. 0.63 ± 0.56) and a more negative binding free-energy estimate (−26.16 ± 2.07 vs. −21.96 ± 1.09 kcal/mol). The dynamic profiles of the remaining complexes are presented in Table 6.

Table 6: Dynamic behavior of selected protein–ligand complexes during molecular dynamics simulations.

Protein Data Bank identifier	Original panels
1J3I	RMSD; RMSF; H-bond; Rg; SASA; MM/GBSA
6UKJ	RMSD; RMSF; H-bond; Rg; SASA; MM/PBSA
4YA8	RMSD; RMSF; H-bond; Rg; SASA; MM/GBSA
2XYG	RMSD; RMSF; H-bond; Rg; SASA; MM/GBSA
6GL8	RMSD; RMSF; H-bond; Rg; SASA; MM/GBSA

RMSD = root-mean-square deviation; RMSF = root-mean-square fluctuation; H-bond = hydrogen-bond; Rg = radius of gyration; SASA = solvent-accessible surface area; MM/GBSA = molecular mechanics/generalized Born surface area. MM/PBSA = Molecular Mechanics/Poisson–Boltzmann Surface Area. Protein Data Bank identifiers: 1J3I = *Plasmodium falciparum* dihydrofolate reductase–thymidylate synthase; 6UKJ = *Plasmodium falciparum* chloroquine resistance transporter; 4YA8 = *Plasmodium falciparum* plasmepsin II; 2XYG = caspase-3; 6GL8 = Bcl-2.

For PMII, 2-coumaroylquinic acid exhibited a lower mean RMSD than artemisinin (7.81 ± 1.68 vs. 20.34 ± 8.28 Å) and a more negative MM/GBSA estimate (−14.83 ± 6.33 vs. −12.16 ± 0.5 kcal/mol). The mean RMSF values were 0.93 ± 0.69 Å for 2-coumaroylquinic acid and 0.84 ± 0.46 Å for artemisinin.

For caspase-3, both 2-coumaroylquinic acid and artemisinin exhibited comparatively low mean RMSD values (2.39 ± 0.23 and 2.68 ± 0.30 Å, respectively). The mean number of hydrogen bonds was higher for 2-coumaroylquinic acid than for artemisinin (1.33 ± 1.18 vs. 0.27 ± 0.54). The corresponding MM/GBSA estimates were −11.15 ± 2.26 and −4.64 ± 1.4 kcal/mol.

For Bcl-2, luteolin exhibited a more negative MM/GBSA estimate than artemisinin (−20.54 ± 0.35 vs. −18.17 ± 1.32 kcal/mol) and a higher mean number of hydrogen bonds (0.78 ± 0.71 vs. 0.24 ± 0.44). However, luteolin also exhibited higher mean RMSD (7.85 ± 1.14 vs. 6.13 ± 1.61 Å) and RMSF (0.97 ± 0.47 vs. 0.82 ± 0.40 Å) values.

Overall, the simulations revealed target-dependent differences in structural deviation, hydrogen-bond interactions, and estimated binding free energies. These findings were derived from single 100-ns trajectories and should therefore be interpreted as preliminary computational observations. Independent simulation replicates and experimental target-validation studies are required to determine their reproducibility and biological relevance.

In silico absorption, distribution, metabolism, excretion, and toxicity (ADMET) evaluation

Of the 33 tentatively identified metabolites, 14 satisfied the stated screening criteria based on Lipinski's rule of five and predicted toxicity classification (Table 7). The selected compounds represented several phytochemical classes, including flavonoids, coumarins, phenolic compounds, dihydrochalcones, and alkaloids.

Table 7: *In silico* ADMET properties and Lipinski's rule of five evaluation of tentatively identified compounds.

No.	Name	Formula	Molecular weight (g/mol)	Phytochemical class	Predicted toxicity class	GI absorption	Bioavailability score	Lipinski
1	Scopoletin	C10 H8 O4	192.17	Coumarin	5	High	0.55	0 violation
2	Morin	C15 H10 O7	302.24	Flavonol	5	High	0.55	0 violation
3	Kaempferol	C15 H10 O6	286.24	Flavonol	5	High	0.55	0 violation
4	Phloretin	C15 H14 O5	274.27	Dihydrochalcone	4	High	0.55	0 violation
5	Trigonelline	C7 H7 N O2	137.14	Alkaloid	5	High	0.55	0 violation
6	Luteolin	C15 H10 O6	286.24	Flavone	5	High	0.55	0 violation
7	4-Hydroxybenzoic acid glucoside	C13 H16 O8	300.26	Phenolic compound	5	Low	0.56	0 violation
8	Isorhamnetin	C16 H12 O7	316.26	Flavonol	5	High	0.55	0 violation
9	Catechin	C15 H14 O6	290.27	Flavan-3-ol	6	High	0.55	0 violation
10	2-Coumaroylquinic acid	C16 H18 O8	338.31	Phenolic/organic acid derivative	5	Low	0.56	0 violation
11	(+)-Epicatechin	C15 H14 O6	290.27	Flavan-3-ol	6	High	0.55	0 violation
12	4-Hydroxybenzoic acid	C7 H6 O3	138.12	Phenolic compound	5	High	0.85	0 violation
13	Naringenin	C15 H12 O5	272.25	Flavanone	4	High	0.55	0 violation
14	o-Hydroxyphenyl-beta-D-glucoside	C12 H16 O7	272.25	Phenolic glycoside	5	High	0.55	0 violation

ADMET = absorption, distribution, metabolism, excretion, and toxicity; GI = gastrointestinal; g/mol = grams per mole. Predicted toxicity classes are computational classifications assigned by ProTox 3.0. Lipinski indicates the number of violations of Lipinski's rule of five. The reported values are computational predictions and do not establish experimental bioavailability or safety.

All 14 selected compounds had zero reported violations of Lipinski's rule of five. Predicted gastrointestinal absorption was high for 12 compounds and low for 4-hydroxybenzoic acid glucoside and 2-coumaroylquinic acid. The reported bioavailability scores ranged from 0.55 to 0.85, and the predicted toxicity classifications ranged from class IV to class VI.

The selected metabolites included morin, kaempferol, luteolin, isorhamnetin, catechin, (+)-epicatechin, and naringenin among the flavonoid-related compounds, together with scopoletin, phloretin, trigonelline, and several phenolic derivatives. These results describe the predicted physicochemical and toxicity characteristics of the screened metabolites. They do not establish oral bioavailability, safety, or antimalarial efficacy in experimental animals or humans.

In vivo antimalarial activity

The antimalarial activity of *A. indica* leaf extract was assessed by measuring parasitemia and percentage suppression (Table 8). One-way analysis of variance demonstrated a statistically significant overall difference in parasitemia among the experimental groups ($p < 0.001$).

Mean parasitemia was highest in the NC group (38.83 ± 13.79%) and lowest in the artesunate-treated group (1.65 ± 0.99%). Mean parasitemia in mice receiving *A. indica* extract at 250, 500, and 750 mg/kg body weight was 8.50 ± 5.49%, 6.96 ± 3.13%, and 9.00 ± 3.14%, respectively.

Parasitemia suppression was 78.11 ± 14.13%, 82.08 ± 8.06%, and 76.83 ± 8.09% at extract doses of 250, 500, and 750 mg/kg body weight, respectively, compared with 95.75 ± 2.56% in the artesunate-treated group. The highest numerical suppression among the extract-treated groups occurred at 500 mg/kg body weight.

Table 8: Mean and standard deviations of parasitemia and suppression in the control and treatment groups.

Group	Parasitemia (mean ± SD)	Statistical comparison	Suppression (%) (mean ± SD)	Statistical comparison	p-value (ANOVA)
NC (negative control)	38.83 ± 13.79	a	0	a	0.05
PC (artesunate, 2.4 mg/kg BW)	1.65 ± 0.99	b	95.75 ± 2.56	b	
T1 (250 mg/kg BW)	8.50 ± 5.49	b	78.11 ± 14.13	b	
T2 (500 mg/kg BW)	6.96 ± 3.13	b	82.08 ± 8.06	b	
T3 (750 mg/kg BW)	9.00 ± 3.14	b	76.83 ± 8.09	b	

NC = negative control; PC = artesunate, 2.4 mg/kg BW; T1 = 250 mg/kg BW; T2 = 500 mg/kg BW; T3 = 750 mg/kg BW. Values are presented as mean ± SD. The analysis of variance (ANOVA) p-value represents the overall comparison among groups using one-way ANOVA. Different superscript letters indicate statistically significant differences according to Tukey's post hoc test ($p < 0.05$). Groups sharing the same superscript are not significantly different.

Nevertheless, the numerical suppression values were lower in all extract-treated groups than in the artesunate-treated group. The absence of a statistically significant difference does not establish equivalent antimalarial efficacy.

The results show parasitemia suppression after administering *A. indica* leaf extract in the chloroquine-sensitive *P. berghei* model, with the highest numerical suppression at 500 mg/kg body weight. The experimental findings do not establish the activity of individual metabolites or the molecular mechanisms underlying the observed suppression.

DISCUSSION

Metabolomic profiling and potential antimalarial mechanisms

Untargeted LC-HRMS analysis tentatively identified 33 metabolites in the *A. indica* leaf extract. These constituents represented several phytochemical classes, including coumarins, flavonol glycosides, flavonols, dihydrochalcones, flavan-3-ols, flavones, flavanones, alkaloids, and phenolic derivatives. The chemical diversity of the extract provides a basis for investigating potential interactions with multiple biological pathways. However, the detection of these compounds does not establish their individual contributions to the observed antimalarial activity.

Artemisinin and related antimalarial agents are associated with oxidative processes that contribute to parasite killing, whereas artemisinin-resistant parasites may exhibit altered responses to oxidative damage [17, 18]. Several polyphenols tentatively identified in the extract, including quercetin, rutin, kaempferol, and myricetin, possess hydroxylated aromatic structures associated with electron-transfer and radical-scavenging properties *in vitro* [19]. These characteristics raise the hypothesis that constituents of the extract could influence oxidative processes in the parasite or host. Nevertheless, the present study did not measure reactive oxygen species, antioxidant activity, or parasite oxidative-stress responses. Consequently, an oxidative mechanism cannot be inferred from the metabolomic profile alone.

Changes in parasite transport proteins, including PfCRT and *P. falciparum* multidrug resistance protein 1 (PfMDR1), have been associated with altered susceptibility to antimalarial drugs [20, 21]. Flavonoids such as quercetin, luteolin, and naringenin have also been investigated for their interactions with membrane-associated transport systems and membrane lipids [22]. These observations provide a rationale for examining whether the identified metabolites interact with parasite transport proteins. However, the present study did not measure transporter activity, intracellular drug accumulation, or the susceptibility of drug-resistant parasites. Any potential effect on antimalarial drug transport therefore remains hypothetical.

The simultaneous detection of scopoletin, rutin, isoquercetin, phenolic acids, and other constituents also raises the possibility of additive or synergistic effects within the crude extract. Such interactions cannot be established from chemical profiling or whole-extract activity alone. Testing this hypothesis would require quantification of individual metabolites, bioassay-guided fractionation, and controlled experiments involving purified compounds and defined combinations.

Future studies should quantify major constituents, including scopoletin, rutin, and isoquercetin, using authentic analytical standards. The antimalarial activity of isolated compounds and their combinations should then be evaluated against characterized artemisinin-sensitive and artemisinin-resistant *P. falciparum* strains, including strains carrying relevant *Kelch13* mutations. Ring-stage survival assays and formal drug-interaction analyses, including isobologram-based fractional inhibitory concentration measurements, could help distinguish individual activity from additive, synergistic, or antagonistic effects.

Molecular docking and target-specific interaction hypotheses

Molecular docking was used to investigate the predicted interactions of selected metabolites with PfDHFR-TS, PfCRT, PMII, caspase-3, and Bcl-2. The inclusion of parasite-associated targets and host apoptotic regulators allowed the exploration of distinct interaction hypotheses. However, docking scores represent computational estimates of ligand-binding and cannot independently demonstrate enzyme inhibition, transporter modulation, or changes in host-cell signaling.

Luteolin exhibited a favorable predicted interaction with PfCRT, with a docking score of −8.827 kcal/mol compared with −8.204 kcal/mol for artemisinin. PfCRT is associated with antimalarial drug transport and altered drug susceptibility, making it a relevant target for exploratory computational studies. Previous docking and MD investigations have reported predicted interactions between phytochemicals and regions associated with the PfCRT transport pathway [25]. These findings are consistent with ligand association with this transporter. Nevertheless, the predicted interaction does not establish that luteolin inhibits transport, increases intracellular antimalarial concentrations, or reverses drug resistance. These possibilities require functional transport assays and susceptibility testing.

Catechin exhibited a predicted binding energy of −8.672 kcal/mol against PfDHFR-TS, compared with −8.197 kcal/mol for artemisinin. The modeled catechin complex included hydrogen-bond interactions with Asp54, Ser101, and Tyr160. Previous investigations have reported interactions between catechin derivatives and dihydrofolate reductase, with inhibitory activity influenced by compound structure [26]. A docking study involving phytoconstituents of *Cannabis sativa* also evaluated catechin against PfDHFR-TS and reported favorable predicted binding relative to pyrimethamine [27]. These findings support further examination of catechin as a potential ligand, but a more negative docking score does not establish greater inhibitory potency. Direct enzyme inhibition assays are necessary to determine whether the predicted interactions have functional consequences.

For PMII, 2-coumaroylquinic acid exhibited a predicted binding energy of −7.560 kcal/mol, compared with −6.520 kcal/mol for artemisinin. Plasmepsin II has been investigated as a potential antimalarial target, including in phytochemical docking studies [10]. The predicted interaction of 2-coumaroylquinic acid with the modeled binding pocket provides a basis for subsequent enzymatic investigation. However, the present findings do not establish inhibition of plasmepsin II or disruption of parasite hemoglobin metabolism.

The exploratory docking results for caspase-3 and Bcl-2 require a separate interpretation because these proteins are associated with host-cell responses rather than direct parasite-specific activity. Severe malaria can involve inflammatory injury and altered host-cell survival pathways [23], and previous experimental work has investigated the effects of caspase inhibition in murine models [13]. Luteolin showed a predicted binding energy of −6.927 kcal/mol with Bcl-2, whereas 2-coumaroylquinic acid showed a predicted binding energy of −6.682 kcal/mol with caspase-3. Although modulation of BCL-2-associated pathways can produce important biological effects, the consequences depend on the cellular and disease context [24]. The present docking results cannot determine whether these ligands activate or inhibit the respective proteins, alter apoptosis, or protect host tissues.

Accordingly, the molecular docking findings should be regarded as a prioritization framework for subsequent functional studies rather than confirmation of a multi-target antimalarial mechanism.

LE and molecular recognition

Predicted binding energy can be influenced by ligand size because larger molecules may form more contacts within a binding pocket. LE was therefore considered alongside docking scores to provide a size-normalized description of predicted molecular recognition.

Artemisinin exhibited LE values of 0.431 and 0.432 against PfDHFR-TS and PfCRT, respectively. These values were comparable to or higher than those of several screened metabolites, despite artemisinin not always exhibiting the most negative docking score. For example, catechin had a more negative predicted binding energy than artemisinin against PfDHFR-TS but a lower LE value (0.413 vs. 0.431). Similarly, luteolin exhibited a more negative predicted binding energy against PfCRT but a slightly lower LE value (0.420 vs. 0.432).

These comparisons illustrate why docking scores and LE metrics should be considered together. A more negative predicted binding energy may partly reflect ligand size rather than a proportionate increase in binding efficiency. Nevertheless, LE remains a computational descriptor and does not establish experimental affinity, target inhibition, or antimalarial potency.

MD simulations and binding stability

MD simulations provided additional information on the modeled behavior of selected protein–ligand complexes over 100 ns. The combined assessment of RMSD, RMSF, hydrogen-bond interactions, Rg, SASA, and estimated binding free energies revealed target-dependent differences between the selected metabolites and artemisinin.

In the PfDHFR-TS system, catechin showed lower mean RMSD and RMSF than artemisinin, along with a higher mean number of hydrogen bonds. Its MM/GBSA estimate was also slightly more negative (−23.49 ± 2.82 vs. −22.63 ± 1.71 kcal/mol). These observations suggest that catechin maintained a comparatively consistent modeled interaction with PfDHFR-TS under the simulated conditions. However, the difference in estimated binding free-energy was small relative to the reported variability, and the results do not establish stronger experimental binding or greater enzymatic inhibition.

The luteolin–PfCRT complex exhibited a lower mean RMSD than the artemisinin–PfCRT complex (1.98 ± 0.65 vs. 5.36 ± 1.34 Å). Luteolin also showed a higher mean number of hydrogen bonds and a more negative estimated binding free-energy. These results indicate differences in the simulated structural behavior of the two complexes. They do not demonstrate inhibition of chloroquine transport or restoration of drug susceptibility. Functional transport measurements and parasite susceptibility assays are required to evaluate those possibilities.

For PMII, the complex containing 2-coumaroylquinic acid exhibited a lower mean RMSD than the artemisinin complex (7.81 ± 1.68 vs. 20.34 ± 8.28 Å). Its estimated binding free-energy was also more negative (−14.83 ± 6.33 vs. −12.16 ± 0.5 kcal/mol). However, the substantial variability in the estimate for 2-coumaroylquinic acid limits interpretation of the energetic difference. Further simulations and direct plasmepsin inhibition assays are necessary before drawing conclusions about functional target engagement.

The simulations involving caspase-3 and Bcl-2 similarly revealed differences in modeled interactions without establishing their biological consequences. The caspase-3–2-coumaroylquinic acid complex exhibited a higher mean number of hydrogen bonds and a more negative estimated binding free-energy than the corresponding artemisinin complex. In the Bcl-2 system, luteolin exhibited a more negative estimated binding free-energy and more frequent hydrogen-bond interactions than artemisinin, but its higher RMSD and RMSF values indicated greater conformational variation during the simulation. These findings do not demonstrate caspase-3 inhibition, Bcl-2 modulation, or altered host-cell apoptosis.

The interpretation of all MD results is constrained by the use of a single 100-ns trajectory for each complex. Without independent simulation replicates, it is difficult to distinguish reproducible interaction patterns from trajectory-specific behavior. Moreover, structural persistence in a simulation does not directly translate into enzyme inhibition constants, effective concentrations, duration of action, or therapeutic efficacy. Longer simulations, replicate trajectories, and experimental target assays are needed to validate the observed computational trends.

Predicted pharmacokinetic properties and toxicity

The *in silico* ADMET analysis provided preliminary information on the physicochemical, absorption-related, and toxicity characteristics of the selected metabolites. Fourteen compounds satisfied the stated screening criteria, and all had zero reported violations of Lipinski's rule of five. Most compounds were predicted to have high gastrointestinal absorption, whereas 4-hydroxybenzoic acid glucoside and 2-coumaroylquinic acid were predicted to have low gastrointestinal absorption.

Differences in molecular size, polarity, and structural complexity may contribute to the variation in predicted pharmacokinetic properties. For example, 4-hydroxybenzoic acid had a reported bioavailability score of 0.85, whereas most other selected compounds had scores of 0.55 or 0.56. However, these scores are computational predictions rather than measured oral bioavailability.

The predicted toxicity classes also provide only preliminary screening information. The classification of a compound within a particular predicted toxicity category does not establish its safety in laboratory animals or humans. Experimental studies are required to evaluate systemic exposure, metabolism, dose-dependent toxicity, and potential interactions among extract constituents.

The chemical diversity of the extract raises the possibility that several metabolites contribute to its overall biological activity. Nevertheless, the present study did not quantify systemic exposure to individual constituents or establish pharmacological interactions among them. The data therefore do not demonstrate synergy, a defined polypharmacological mechanism, or a reduced likelihood of resistance development.

In vivo antimalarial activity

The *in vivo* findings showed parasitemia suppression after administering *A. indica* leaf extract to mice infected with chloroquine-sensitive *P. berghei* ANKA. Suppression was 78.11 ± 14.13%, 82.08 ± 8.06%, and 76.83 ± 8.09% at 250, 500, and 750 mg/kg body weight, respectively. The highest numerical suppression occurred at 500 mg/kg body weight, whereas artesunate produced 95.75 ± 2.56% suppression.

Overall, the experimental groups differed significantly ($p < 0.001$). The extract-treated groups had lower parasitemia than the NC group. However, the absence of statistically significant pairwise differences between the extract-treated groups and the artesunate-treated group does not demonstrate therapeutic equivalence. The study was not designed to establish non-inferiority or equivalence, and the extract consistently achieved lower suppression than artesunate.

The absence of a monotonic dose–response relationship is also notable. Increasing the extract dose from 500 to 750 mg/kg body weight did not increase parasitemia suppression. This pattern may reflect biological variability, differences in extract constituent disposition, or other factors, but the present data do not identify the cause. The small number of animals per group further limits the precision of dose–response comparisons.

Previous studies have also investigated the antimalarial potential of *A. indica* preparations. Rahmah *et al.* [4] reported parasitemia reductions of approximately 67.06% to 73.27%. using a leaf extract in a *P. berghei* mouse model. Differences in extraction solvent, dose, mouse strain, and experimental procedures may affect comparisons with the present findings. However, these methodological differences alone cannot explain variation in antimalarial activity without comparative chemical and pharmacological measurements.

Faloye *et al.* [28] reported parasite suppression using an ethanolic fruit extract at a higher administered dose. Because fruit and leaf preparations may differ substantially in chemical composition, their results should not be treated as directly interchangeable. Similarly, Somsak *et al.* [29] investigated the effects of an aqueous leaf preparation in *P. berghei*-infected mice, including outcomes related to malaria-associated kidney injury. These findings provide context for broader investigations of neem preparations but do not establish that the extract evaluated in the present study protects against organ injury.

Adoley *et al.* [30] investigated the *in vitro* antiplasmodial activity of a preparation combining *A. indica* and *Khaya senegalensis* against chloroquine-sensitive and chloroquine-resistant *P. falciparum* strains. These findings concern a different preparation and experimental system. *In vitro* parasite assays can help characterize direct antiplasmodial activity, whereas *in vivo* studies additionally involve host metabolism, systemic exposure, immune responses, and other physiological factors. Consequently, activity observed in one model cannot be assumed to translate directly to another.

The present findings support further investigation of the antimalarial activity of *A. indica* leaf extract. However, they do not identify the active constituents responsible for parasitemia suppression or demonstrate efficacy against artemisinin-resistant parasites. Studies using standardized extracts, purified fractions, defined parasite strains, and pharmacokinetic measurements are needed to clarify the relationship between extract composition and biological activity.

Methodological strengths, limitations, and future directions

A strength of the study was its integration of chemical profiling, computational screening, and an experimental rodent malaria model. Using a single homogenized extract batch for chemical characterization and *in vivo* evaluation provided a common material basis for the different components of the investigation. The computational analyses also generated specific ligand–target hypotheses that can guide subsequent experiments.

Several limitations must be considered. First, LC-HRMS annotations were tentative and were not confirmed through comparison with authentic analytical standards. The relative chromatographic peak areas do not provide absolute concentrations or establish the quantities of individual metabolites administered to the animals.

Second, the molecular docking and MD analyses were predictive. The study did not measure direct inhibition of PfDHFR-TS or PMII, PfCRT transport activity, or functional modulation of caspase-3 and Bcl-2. In addition, the MD simulations used single 100-ns trajectories, limiting assessment of the reproducibility of the modeled interaction patterns.

Third, the *in vivo* evaluation used a chloroquine-sensitive rodent parasite strain. The findings therefore cannot establish activity against drug-resistant *P. falciparum* or reversal of artemisinin resistance. The study also used five mice per group, which limited the precision of comparisons among extract doses and between extract treatment and artesunate. The absence of a statistically significant difference between these treatments must not be interpreted as evidence of equivalent efficacy.

Fourth, the study did not establish the systemic bioavailability of the tentatively identified metabolites. The predicted ADMET characteristics were not validated experimentally, and the contributions of individual compounds or compound combinations to the observed parasitemia suppression remain unknown.

Finally, liver function markers, histopathological outcomes, and experimental measures of apoptosis were not assessed. Accordingly, the computational observations involving host apoptotic regulators do not support conclusions about host-tissue protection.

Future investigations should include quantitative chemical standardization, bioassay-guided fractionation, direct target-inhibition assays, and experimental pharmacokinetic and toxicity studies. Evaluation against well-characterized drug-sensitive and drug-resistant *P. falciparum* strains would help determine whether the observed activity extends beyond the rodent model. Independent MD replicates, larger animal cohorts, and appropriately designed comparative efficacy studies would further strengthen the evidence.

Taken together, the findings establish an initial experimental and computational basis for investigating the antimalarial potential of *A. indica* leaf extract. The chemical profiling identifies candidate metabolites, the computational analyses suggest possible ligand–target interactions, and the rodent study demonstrates parasitemia suppression under the tested conditions. The relationships among these observations remain to be established through targeted experimental validation.

CONCLUSION

This study integrated LC-HRMS metabolomic profiling, *in silico* analyses, and *in vivo* antimalarial evaluation to investigate the potential of *A. indica* leaf extract. Metabolomic profiling tentatively identified 33 compounds representing several phytochemical classes, with scopoletin showing the largest reported chromatographic peak area. Molecular docking and MD simulations identified target-specific interaction patterns involving catechin with PfDHFR-TS, luteolin with PfCRT, and 2-coumaroylquinic acid with PMII. These computational findings provide preliminary hypotheses for further investigation but do not establish direct inhibition of the respective targets.

In the chloroquine-sensitive *P. berghei* model, the extract suppressed parasitemia by 78.11%, 82.08%, and 76.83% at doses of 250, 500, and 750 mg/kg body weight, respectively. The highest numerical suppression occurred at 500 mg/kg body weight, whereas artesunate produced 95.75% suppression. Although pairwise comparisons did not identify statistically significant differences between the extract-treated and artesunate-treated groups, this finding does not establish equivalent efficacy.

The results provide a basis for prioritizing selected constituents of *A. indica* for further antimalarial investigation. Combining chemical profiling with computational screening may help guide the selection of compounds for direct biological testing. However, the activity of the crude extract cannot be attributed to individual metabolites without experimental confirmation. The findings do not support replacing established antimalarial treatment with the extract.

A. indica leaf extract demonstrated antimalarial activity in a chloroquine-sensitive rodent malaria model, while metabolomic and computational analyses identified constituents and molecular interactions warranting further investigation. The findings support continued experimental evaluation of the extract and its metabolites but do not establish their individual mechanisms of action, clinical efficacy, or suitability as alternatives to established antimalarial therapies.

DATA AVAILABILITY

The sets of data obtained and analyzed from this research are available from the corresponding author upon request.

GENERATIVE AI DECLARATION

Google Translate and Gemini Edu were used solely for language editing and improving the grammar and readability of the manuscript. The generated content was critically reviewed, revised, and verified by the authors. All experimental design, data collection, analysis, interpretation, and conclusions were performed by the authors, who assume full responsibility for the content of the article. No artificial intelligence tool was credited as an author.

AUTHORS' CONTRIBUTIONS

DAASL: Conceived and designed the study. DAASL, PIBA, and IGKNA: Conducted the *in vivo* experiments.

MBP: Performed molecular docking and molecular dynamics simulations. DAASL, PIBA, MBP, and IKT: Analyzed and interpreted the data. DAASL and IMAGW: Analyzed and interpreted the data and revised the manuscript. All authors have read and approved the final version of the manuscript.

ACKNOWLEDGMENTS

The authors thank the Dean of the Faculty of Medicine, Udayana University, for providing the facilities and support necessary to conduct this research at the Integrated Biomedical Laboratory. This research received no external financial support from any public, commercial, or not-for-profit funding agency.

COMPETING INTERESTS

The authors declare that they have no competing interests.

PUBLISHER'S NOTE

Veterinary World remains neutral with regard to jurisdictional claims in the published institutional affiliations.

REFERENCES

1. World Health Organization. World malaria report 2025: addressing the threat of antimalarial drug resistance. Geneva: World Health Organization; 2025 [Cited 12 April 2026]. Available from: https://cdn.who.int/ media/ docs/default-source/malaria/world-malaria-reports/world-malaria-report-2025-partner-briefing-eng.pdf.
2. Menard D, Dondorp A. Antimalarial drug resistance: a threat to malaria elimination. Cold Spring Harb Perspect Med. 2017;7(7):1–24.
3. Laksemi DAAS, Sukrama IDM, Suwanti LT, Sudarmaja IM, Damayanti PAA, Tunas IK, *et al.* A comprehensive review on medicinal plants potentially as antimalarial. Trop J Nat Prod Res. 2022;6(3):287–298.
4. Rahmah Z, Nirmala KC, Nashichuddin A, Riskiyana R, Milliana A, Indriana N, *et al.* Effect of neem leaf extract (*Azadirachta indica*) in reducing the degree of parasitemia and apoptosis in C57BL mice with cerebral malaria. Vet World. 2024;17(7):1497–1503.
5. Rauf A, Olatunde A, Akram Z, Hemeg HA, Khalil AA, Shariati MA, *et al.* Metabolomic-based promising technique for fruit-based natural products analysis. Food Chem X. 2025;32:1–16.
6. Aghajani J, Farnia P, Farnia P, Ghanavi J, Velayati AA. Molecular dynamic simulations and molecular docking as a potential way for designed new inhibitor drug without resistance. Tanaffos. 2022;21(1):1–14.
7. Mazri R, Ouassaf M, Zekri A, Khan SU, Rengasamy KRR, Alhatlani BY. *In silico* network pharmacology, molecular docking, and molecular dynamics analysis of rosemary-derived compounds as potential HSP90 inhibitors for cancer therapy. Curr Issues Mol Biol. 2025;18:1–23.
8. Laksemi DAAS, Primayanti IDAID, Surudarma IW, Damayanti PAA, Susanti NMP. Antimalarial flavonoid glycoside from *Carica papaya* with inhibitory potential against *Plasmodium falciparum* dihydrofolate reductase–thymidylate synthase: an *in silico* study. Univ Med. 2025;44(1):26–33.
9. Chike-Ekwughe A, Abdulameed HT, Adebayo-Gege GI, Usman A, Omoyungbo EJ, Ala AA, *et al.* Molecular modeling of the interactions of compounds of *Irvingia wombulu* against dihydrofolate reductase-thymidylate synthase in *Plasmodium falciparum* towards development of antimalarial drug. In Silico Pharmacol. 2025;13(1):1–18.
10. Nasamu AS, Polino AJ, Istvan ES, Goldberg DE. Malaria parasite plasmepsins: more than just plain old degradative pepsins. J Biol Chem. 2020;295(25):8425–8441.
11. Small-Saunders JL, Hagenah LM, Fidock DA. Turning the tide: targeting PfCRT to combat drug-resistant *P. falciparum*? Nat Rev Microbiol. 2020;18(5):261–262.
12. Guha M, Kumar S, Choubey V, Maity P, Bandyopadhyay U. Apoptosis in liver during malaria: role of oxidative stress and implication of mitochondrial pathway. FASEB J. 2006;20(8):1224–1226.
13. Sercundes MK, Ortolan LS, da Silva Julio V, Bella LM, de Castro Quirino T, Debone D, *et al.* Blockade of caspase cascade overcomes malaria-associated acute respiratory distress syndrome in mice. Cell Death Dis. 2022;13(2):144.
14. Nissink JWM. Simple size-independent measure of ligand efficiency. J. Chem. Inf. Model. 2009;49(6):1617–1622.

15. Arifin WN, Zahiruddin WM. Sample size calculation in animal studies using resource equation approach. Malays J Med Sci. 2017;24(5):101–105.
16. Habte G, Habte S, Jilo O, Alemu W, Eyasu K, Meka W, *et al*. Antimalarial efficacy test of the aqueous crude leaf extract of *Coriandrum sativum* Linn.: an *in vivo* multiple model experimental study in mice infected with *Plasmodium berghei*. BMC Complement Med Ther. 2024;24(1):267.
17. Egwu CO, Pério P, Augereau JM, Tsamesidis I, Benoit-Vical F, Reybier K. Resistance to artemisinin in falciparum malaria parasites: a redox-mediated phenomenon. Free Radic Biol Med. 2022;179:317–327.
18. Rocamora F, Zhu L, Liong KY, Dondorp A, Miotto O, Mok S, *et al*. Oxidative stress and protein damage responses mediate artemisinin resistance in malaria parasites. PLoS Pathog. 2018;14(3):1–29.
19. Olszowy-Tomczyk M, Wianowska D. Antioxidant properties of selected flavonoids in binary mixtures—considerations on myricetin, kaempferol and quercetin. Int J Mol Sci. 2023;24(12):1–14.
20. Silva M, Malmberg M, Otienoburu SD, Björkman A, Ngasala B, Mårtensson A, *et al*. *Plasmodium falciparum* drug resistance genes *pfmdr1* and *pfcrt in vivo* co-expression during artemether-lumefantrine therapy. Front Pharmacol. 2022;13:1–19.
21. Wicht KJ, Mok S, Fidock DA. Molecular mechanisms of drug resistance in *Plasmodium falciparum* malaria. Annu Rev Microbiol. 2020;74:431–454.
22. Mohana S, Ganesan M, Agilan B, Karthikeyan R, Srithar G, Beaulah Mary R, *et al*. Screening dietary flavonoids for the reversal of P-glycoprotein-mediated multidrug resistance in cancer. Mol Biosyst. 2016;12(8):2458–2470.
23. Vasquez M, Zuniga M, Rodriguez A. Oxidative stress and pathogenesis in malaria. Front Cell Infect Microbiol. 2021;11:1–8.
24. Fowler-Shorten DJ, Hellmich C, Markham M, Bowles KM, Rushworth SA. BCL-2 inhibition in haematological malignancies: clinical application and complications. Blood Rev. 2024;65:1–11.
25. Patel SK, Khedkar VM, Jha PC, Jasrai YT, Pandya HA, George LB, *et al*. Molecular interaction of selected phytochemicals under the charged environment of *Plasmodium falciparum* chloroquine resistance transporter (PfCRT) model. J Biomol Struct Dyn. 2016;34(2):290–303.
26. Sáez-Ayala M, Fernández-Pérez MP, Chazarra S, Mchedlishvili N, Tárraga-Tomás A, Rodríguez-López JN. Factors influencing the antifolate activity of synthetic tea-derived catechins. Molecules. 2013;18(7):8319–8341.
27. David TI, Adelakun NS, Omotuyi OI, Metibemu DS, Ekun OE, Eniafe GO, *et al*. Molecular docking analysis of phyto-constituents from *Cannabis sativa* with PfDHFR. Bioinformation. 2018;14(9):574–579.
28. Faloye KO, Adesida SA, Oguntimehin SA, Adewole AH, Omoyeni OB, Fajobi SJ, *et al*. LC-MS analysis, computational investigation, and antimalarial studies of *Azadirachta indica* fruit. Bioinform Biol Insights. 2023;17:1–9.
29. Somsak V, Chachiyo S, Jaihan U, Nakinchat S. Protective effect of aqueous crude extract of neem (*Azadirachta indica*) leaves on *Plasmodium berghei*-induced renal damage in mice. J Trop Med. 2015;2015:961205.
30. Adoley WA, Johnson R, Boakye-Gyasi ME, Owusu FWA, Obeng LM, Osei-Asibey A, *et al*. Formulation and evaluation of capsules from *Azadirachta indica* and *Khaya senegalensis* for malaria treatment. J Trop Med. 2026;2026:8366410.

****